Supporting Information

Hasson et al. 10.1073/pnas.0903253106

SI Text

Acquisition and Design. Twenty-three participants (10 men and 13 women; mean age = 21.4; SD = 2.6) were recruited from the student population of The University of Chicago. All were right-handed, and had normal hearing and normal (corrected) vision. The study was approved by the Institutional Review Board of the Biological Sciences Division of the University of Chicago, and all participants provided written informed consent.

The experimental materials were made up of 3 types of contents, each consisting of 8 auditory spoken sentences. One-third (20) of the materials were spoken stories in which the final 3 sentences were more informative (MI) given the previous content (i.e., surprising). Another one-third were spoken stories in which the final sentences were less informative (LI) given the previous content (i.e., quite predictable). The final third were nonnarrative sentence (NS) contents that consisted of meaningful sentences that did not make up a continuous meaning. Importantly, the stories in the more- and less-informative conditions were identical apart from a word or two in the third sentence, which determined the informativeness of the 3 critical statements communicated at the end of the story (see ref. 1 for details on stimulus construction). Each story was followed by 22 sec of rest.

Scans were acquired on a 3-Tesla scanner using spiral acquisition with a standard head coil. For each participant, 2 volumetric T1-weighted scans (120 axial slices, 1.5 × 0.938 × 0.938 mm resolution) were acquired and averaged to provide high-resolution images on which to identify anatomical landmarks and onto which functional activation maps could be superimposed. Functional images were acquired in the axial plane (32 slices, slice thickness of 3.8 mm no-gap, interleaved acquisition, matrix size = 64 × 64, TR = 2 sec; TE = 30; flip angle = 77). Effective functional resolution was 3.8 mm^3. We collected 1,620 whole-brain images (216 in each of the first 7 runs, and 108 in the eighth run). An analysis of these data against a synthetic model using general linear models (GLM) has been previously reported in Hasson et al. (1).

Data Analysis: Preprocessing of Individual Functional Data in 3D Space and Projection of Data to 2D Surface. For each subject, images were spatially registered in 3 dimensions to a reference acquisition collected in the first run (using AFNI; ref. 2). The time series (TS) of each of the 8 fMRI runs was intensity scaled to the mean of each voxel. Data were temporally filtered (bandpass; $0.009 < f < 0.08$). We then removed several sources of variance from the TS data via linear regression. These included (*i*) 6 motion parameters estimated during the head motion correction, (*ii*) linear and second-order polynomial trend, and (*iii*) a TS that was generated by averaging the TS of high-intensity white matter voxels (this mask was generated semiautomatically and verified manually). At this stage, data were also corrected for slice-timing differences. No temporal or spatial smoothing was conducted as part of preprocessing in the acquired volumes. Instead, inter-subject registration and smoothing was carried out in the surface domain as detailed below.

The left and right hemispheres of each participant's anatomical volume were inflated to a surface representation and aligned to a common template using the warping procedures implemented in the FreeSurfer software version 3.0.5 (3). The resulting anatomical representations were imported into SUMA (4). This method of group registration in the surface domain results in accurate reflection of individual data at the group level (5), ensures that smoothing avoids inclusion of white matter data, and avoids averaging data across sulci (6). The entire functional TS data of each voxel (in 3D volumetric space) were then projected from the 3D volumes onto the 2D surface. The resulting dataset consisted of 1,620 time points × 196,000 vertexes per hemisphere per participant, and it was in this 2D surface representation that functional connectivity values were established. A 4-mm smoothing kernel was then applied to the TS data to increase the signal-to-noise ratio. In addition, we used FreeSurfer to obtain anatomical parcellations of the cortical surface for each participant. These parcellation methods have been shown to be comparable in accuracy to manual parcellation (7, 8), and their statistical knowledge base derives from a training set incorporating the anatomical conventions of Duvernoy (9).

Data Analysis: Generating Individual-Level Correlation Maps. For each participant, individual-level functional connectivity maps were generated against 2 seed regions (left precuneus, left angular gyrus) in the following manner. First, a reference TS was created by averaging the TSs of all of the vertexes in the seed region (i.e., all vertexes were included independent of their relative activation or deactivation with respect to the experimental task). To minimize the potential effects of motion artifacts on the estimation of connectivity, we removed images acquired during periods where motion exceeded 1 mm (cf. ref. 10). Furthermore, to reduce the potential biasing effects of outlier values in the TS, acquisitions in which the signal values exceeded 5% were replaced with the median of the seed-region TS. All analyses reported in this article were repeated with (*i*) an outlier threshold of 2.5% or (*ii*) no outlier thresholding, and these manipulations resulted in no qualitative changes to the results. We chose left-hemisphere seed regions on the basis of prior use in the literature; recent work suggests that homotopic regions in this network show strong correlations during rest (16), so that choosing right-hemisphere seed regions would have revealed highly similar connectivity maps.

In the second stage, we partitioned the reference TS into 6 TSs, one for each of the states for which we evaluated connectivity. These 6 derived TSs were created by concatenating the relevant acquisitions of interest from the main TS (see ref. 11). We first shifted the time series by 4 sec to account for the delay in the hemodynamic response. This 4-sec shift was performed to capture the portions of the time series associated with the presentation of content of interest. Following this temporal shift, for the analysis of connectivity during language comprehension, we created (for each of the MI, LI, and NS conditions) a TS by concatenating the functional acquisitions associated with the presentation of the final 4 sentences of each story type (8 acquisitions) plus the 3 acquisitions that followed them (i.e., 11 acquisitions; 22 sec). For the analysis of connectivity during the rest periods, we similarly concatenated the acquisitions corresponding to the rest periods that followed the MI, LI, and NS conditions. There were 11 acquisitions associated with the rest period following each story, but, as mentioned, the first 3 of those were analyzed as part of the language time series to account for the attenuation in the hemodynamic response function (HRF) in such contexts, making for 8 rest acquisitions following each story presentation. (Due to the 4-sec shift of the TS and the additional discounting of the first 6 sec of the rest period, the first acquisition treated as a rest period effectively began 10 sec after the preceding story had ended and ended 22 sec later.) We used a peak-fitting algorithm (12) to assess

the return to baseline following story presentation and found it to be within 10−14 sec after the termination of the last sentence.

To establish the temporal synchronization between the reference TS and the TS of each vertex, we computed the cross-correlation between the two. This procedure is similar to establishing a Pearson's product moment of correlation between the 2 TSs, but additionally includes a parameter that accounts for phase (i.e., lag difference) between the series. Given that different brain regions have different HRF dynamics (13, 14), ignoring these systematic phase differences can lead to underestimation of synchronization in case the series are systematically temporally misaligned. In our implementation we limited the lag search window to one acquisition. The cross-correlation function thus established the correlation between the 2 time series for –1, 0, and +1 lag, and the maximal value was taken as the correlation for that vertex. Note that 2 such connectivity maps were created for each condition of interest, one per each seed region.

Data Analysis: Generating Group-Level and Contrast Correlation Maps. Correlation values in each condition were Z transformed using Fisher's transformation, and statistical analyses were carried out on the transformed values. To identify areas showing (*i*) differential FC during listening vs. rest, (*ii*) differential FC as function of language content, or (*iii*) an interaction between the 2 factors, we conducted a 2 (task: listening, rest) × 3 (content: more informative, less informative, nonnarrative) whole-brain ANOVA on a vertex-wise level.

This analysis was conducted twice: once for data corresponding to FC maps generated by the analysis against the precuneus seed region, and once for data generated by the analysis against the angular gyrus seed region. To identify areas showing similar main effects or interaction for both seed regions (e.g., showing a main effect of task in both cases), we identified surface vertexes where the reliability of the effect corresponded to $P < 0.05$ in both analyses. All analyses were conducted against each seed separately to generate single-seed statistical maps, and these were then overlaid to identify regions showing experimental effects in maps defined by both seeds (i.e., the intersection of both statistical maps). In each analysis, the single-voxel threshold for an experimental effect was set at $P < 0.05$. Note that because the time series of the 2 seed regions were not independent (median Pearson's R across participants = 0.5; see supporting information (SI) Fig. S5), the analyses conducted against these seed regions were not independent. That is, if a voxel showed a certain effect when tested against one seed region, there was above-chance likelihood that it would show a similar effect when tested against the other seed region. Because of this interdependence, the joint probability of the 2 tests was not 0.05^2 (.0025) but 0.01. As a result, all tests were controlled for multiple comparisons using a combination of single-voxel threshold of $P < 0.01$ and a cluster extent threshold (all analyses presented were corrected at $P < 0.05$, corrected for family-wise error rate).

To identify areas showing differential FC during rest as a function of preceding context, we conducted a one-way repeated measure ANOVA analyzing FC values for the rest periods that followed the MI, LI, and NS conditions. This analysis was repeated for each seed region separately, and the intersection analysis conducted and thresholded as described. To identify areas where the difference between FC during listening and rest was modulated by content, we identified areas showing a statistically reliable 2 (task: listening vs. rest) × 3 (content: more informative, less informative, nonnarrative sentences) interaction that held for all voxels in these clusters.

To quantify the relation between FC and subsequent memory for the materials, we treated each functional cluster differentiating rest from listening as a functional ROI (fROI). Within each fROI we calculated the mean FC value, for each participant, and correlated those values against participants' subsequent memory scores using a correlation method that is robust against multivariate outliers (using the *robustbase* package of the R statistical language; ref. 15). These analyses were conducted against both seed regions, but we report the results of analyses conducted against the precuneus seed region for the sake of brevity.

1. Hasson U, Nusbaum HC, Small SL (2007) Brain networks subserving the extraction of sentence information and its encoding to memory. *Cereb Cortex* 17:2899–2913.
2. Cox RW (1996) AFNI: Software for analysis and visualization of functional magnetic resonance neuroimages. *Comp Biomed Res* 29(3):162–173.
3. Fischl B, Sereno MI, Dale AM (1999) Cortical surface-based analysis II: Inflation, flattening, and a surface-based coordinate system. *Neuroimage* 9(2):195–207.
4. Saad ZS, et al. (2004) SUMA: An interface for surface-based intra-and inter-subject analysis with AFNI. *IEEE Int Symp Biomed Imaging* 2:1510–1513.
5. Argall BD, Saad ZS, Beauchamp MS (2005) Simplified intersubject averaging on the cortical surface using SUMA. *Hum Brain Mapp* 27(1):14–27.
6. Desai R, Liebenthal E, Possing ET, Waldron E, Binder JR (2005) Volumetric vs. surface-based alignment for localization of auditory cortex activation. *Neuroimage* 26(4):1019–1029.
7. Fischl B, et al. (2004) Automatically parcellating the human cerebral cortex. *Cereb Cortex* 14:11–22.
8. Fischl B, et al. (2002) Whole brain segmentation: Automated labeling of neuroanatomical structures in the human brain. *Neuron* 33:341–355.
9. Duvernoy HM (1991) *The Human Brain: Structure, Three-Dimensional Sectional Anatomy and MRI* (Springer-Verlag, New York).
10. Tian L, et al. (2007) The relationship within and between the extrinsic and intrinsic systems indicated by resting state correlational patterns of sensory cortices. *Neuroimage* 36(3):684–690.
11. Fair DA, et al. (2007) A method for using blocked and event-related fMRI data to study ''resting state'' functional connectivity. *Neuroimage* 35(1):396–405.
12. Skipper JI, Goldin-Meadow S, Small SL (2009) Gestures orchestrate brain networks for language understanding. *Curr Biol* 19:661–667.
13. Formisano E, Goebel R (2003) Tracking cognitive processes with functional MRI mental chronometry. *Curr Opin Neurobiol* 13(2):174–181.
14. Thierry G, Ibarrola D, Demonet JF, Cardebat D (2003) Demand on verbal working memory delays haemodynamic response in the inferior prefrontal cortex. *Hum Brain Mapp* 19(1):37–46.
15. R Development Core Team (2006) R: A language and environment for statistical computing (R Foundation for Statistical Computing, Vienna). Available at http://www.R-project.org/.
16. Stark DE, et al. (2008) Regional variation in interhemispheric coordination of intrinsic hemodynamic fluctuations. *J. Neurosci* 28:13754–13764.

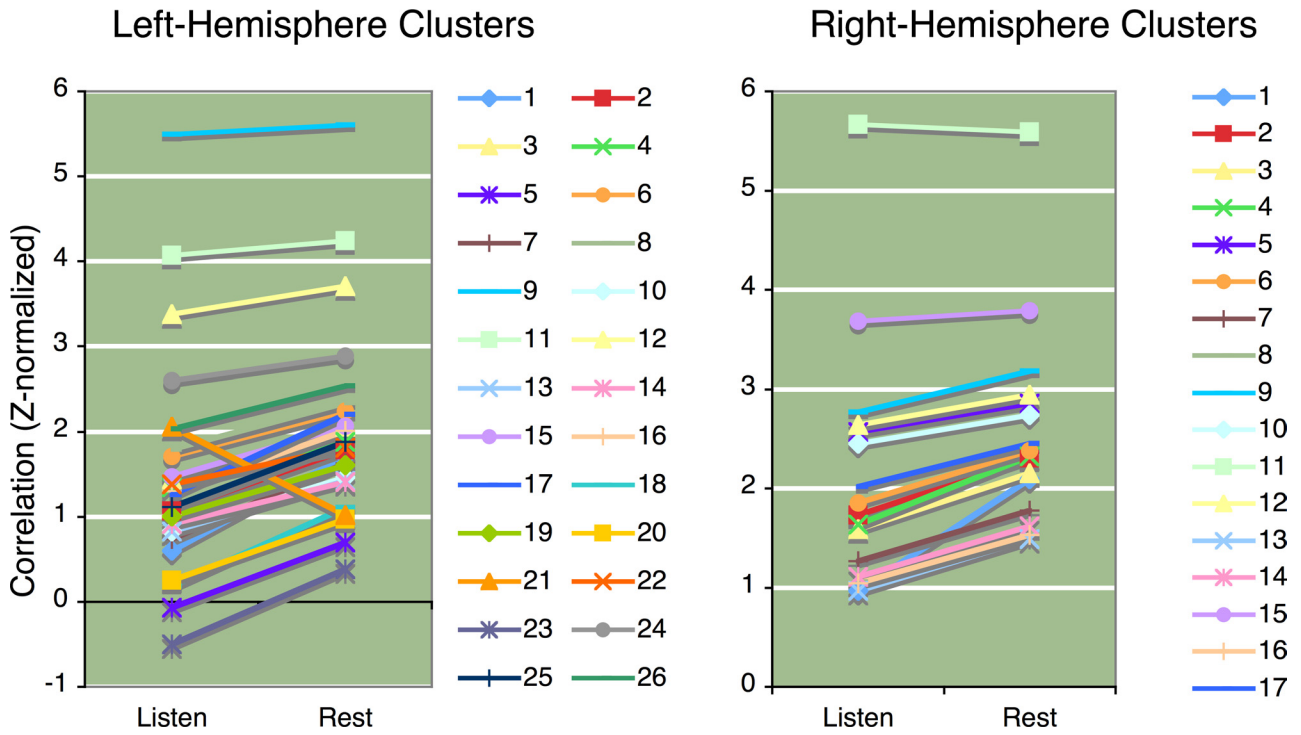

Fig. S1. Magnitude of functional connectivity during listening and rest. The strength of connectivity during listening and rest is displayed for each cluster that differentiated between the two. Numeric indexes match those in Fig. 1 and Table S1. Values reflect connectivity with L. precuneus seed region (highly similar values were found when tested against L. angular G. seed region, not shown).

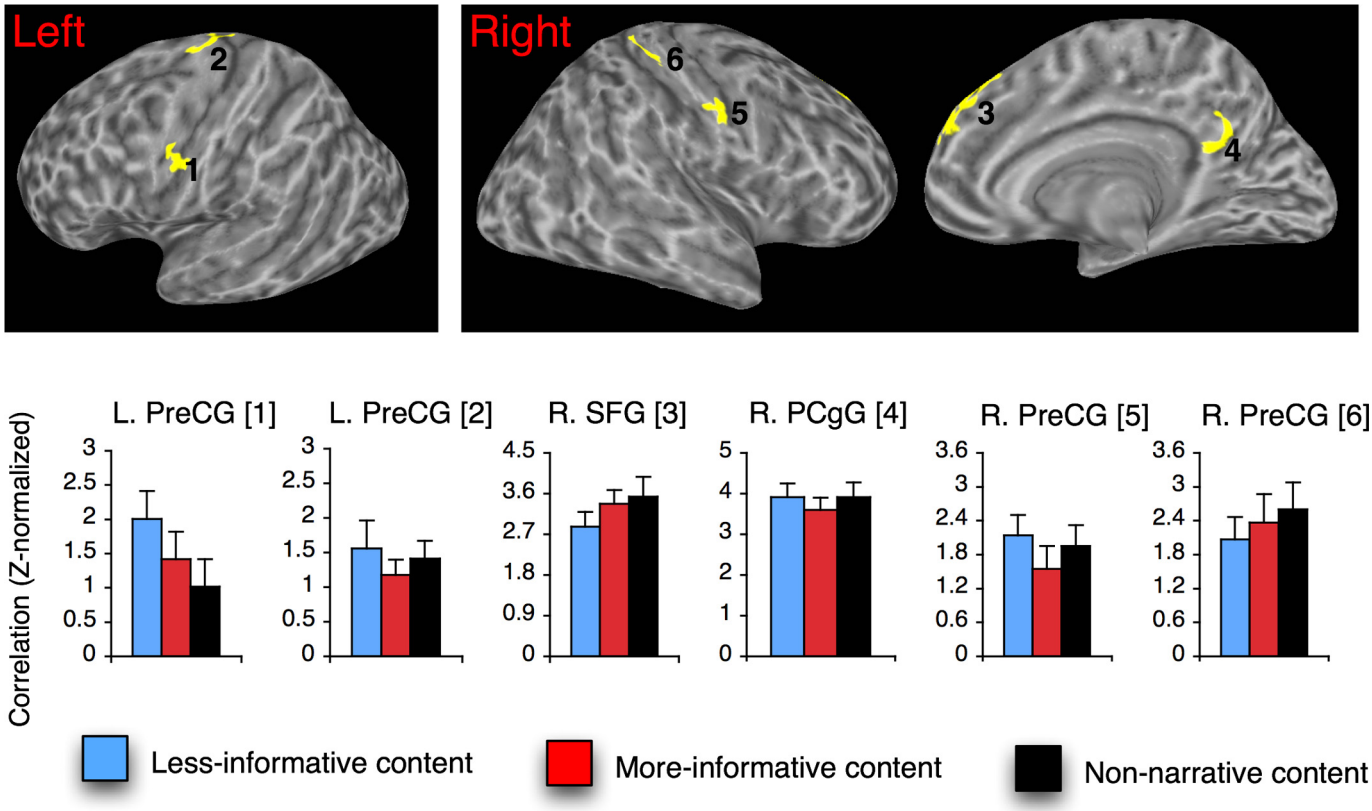

Fig. S2. Regions in which functional connectivity during rest varied as function of preceding content. Values reflect connectivity with L. precuneus seed region (highly similar values found when tested against L. angular G. seed region, not shown). Standard error bars indicate the SE of the mean across participants. PreCG, precentral G.; SFG, superior frontal G.; PCgG, posterior cingulate G.

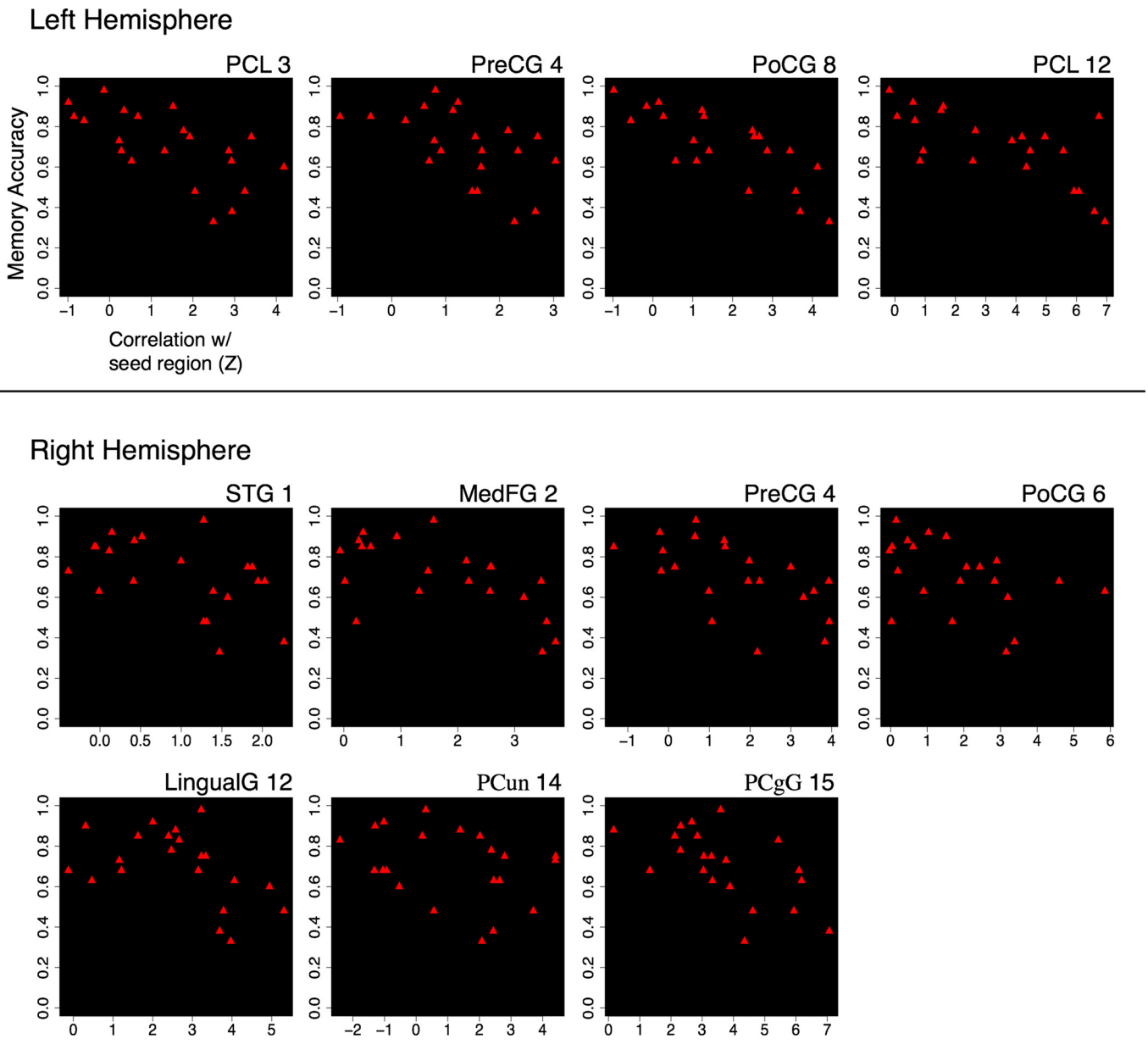

Fig. S3. Interindividual differences in functional connectivity during listening predict subsequent memory for content. Of the functional clusters that showed differential connectivity between listening and rest periods (Fig. 1), 11 demonstrated a reliable association between participants' FC value during listening and their memory for language content (minimal correlation P value $< .004$, after FDR correction for multiple comparisons). The figure presents correlation against L. precuneus seed region. Cluster indexes match those in Fig. 1 and Table S1. PCL, paracentral lobule; MedFG, medial frontal G; PCun, precuneus. Other abbreviations as in Fig. S2.

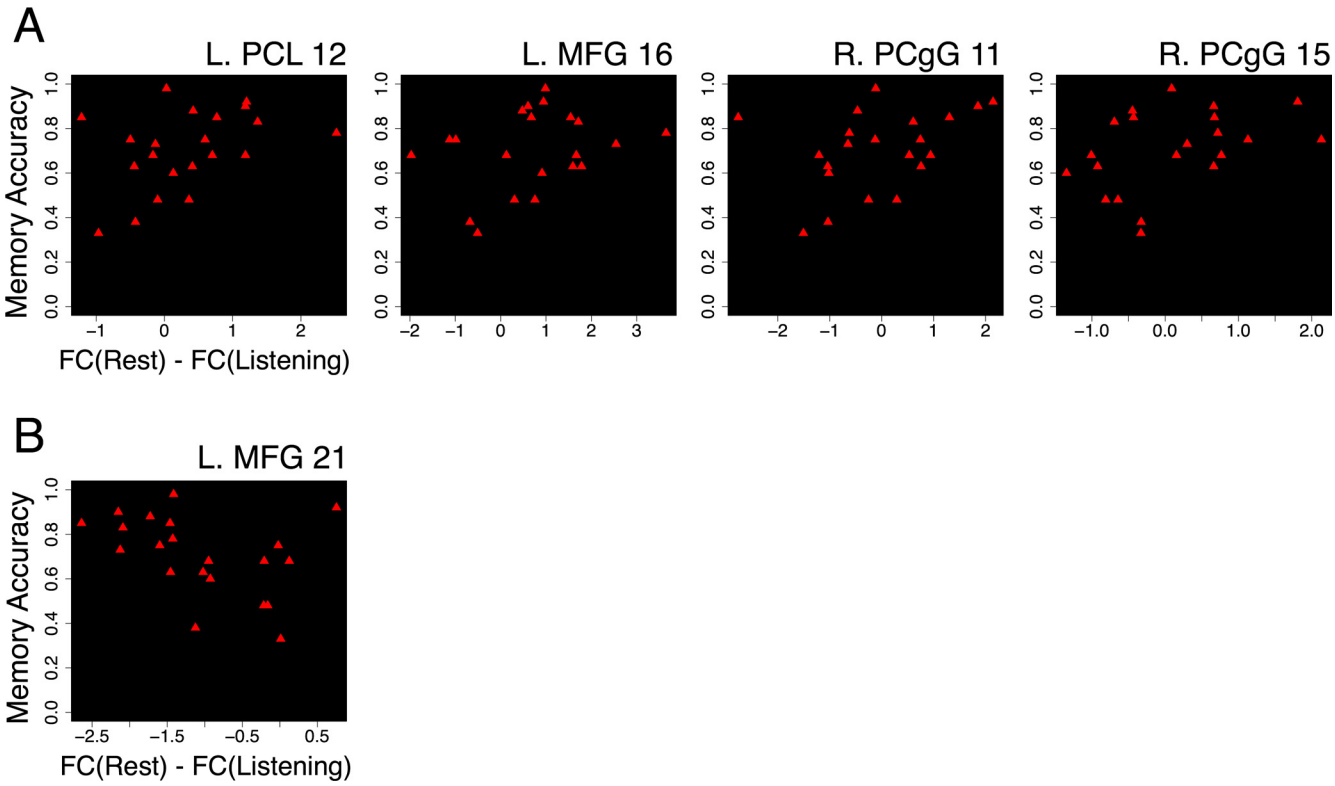

Fig. S4. Shifts in magnitudes of functional connectivity predict subsequent memory for content. Of the functional clusters that showed differential connectivity between listening and rest periods (Fig. 1), 5 demonstrated a relation between the degree of shift in FC between rest and listening [FC(rest) − FC(listening)] and subsequent memory for the story materials. The figure presents correlation against L. precuneus seed region. Cluster indexes match those in Figure S1 and Table S1. (*A*) Regions where FC during rest was greater than FC during task. (*B*) One of only 2 regions where FC was higher during listening than during rest. MFG, middle frontal G; other abbreviations as in Fig. S3.

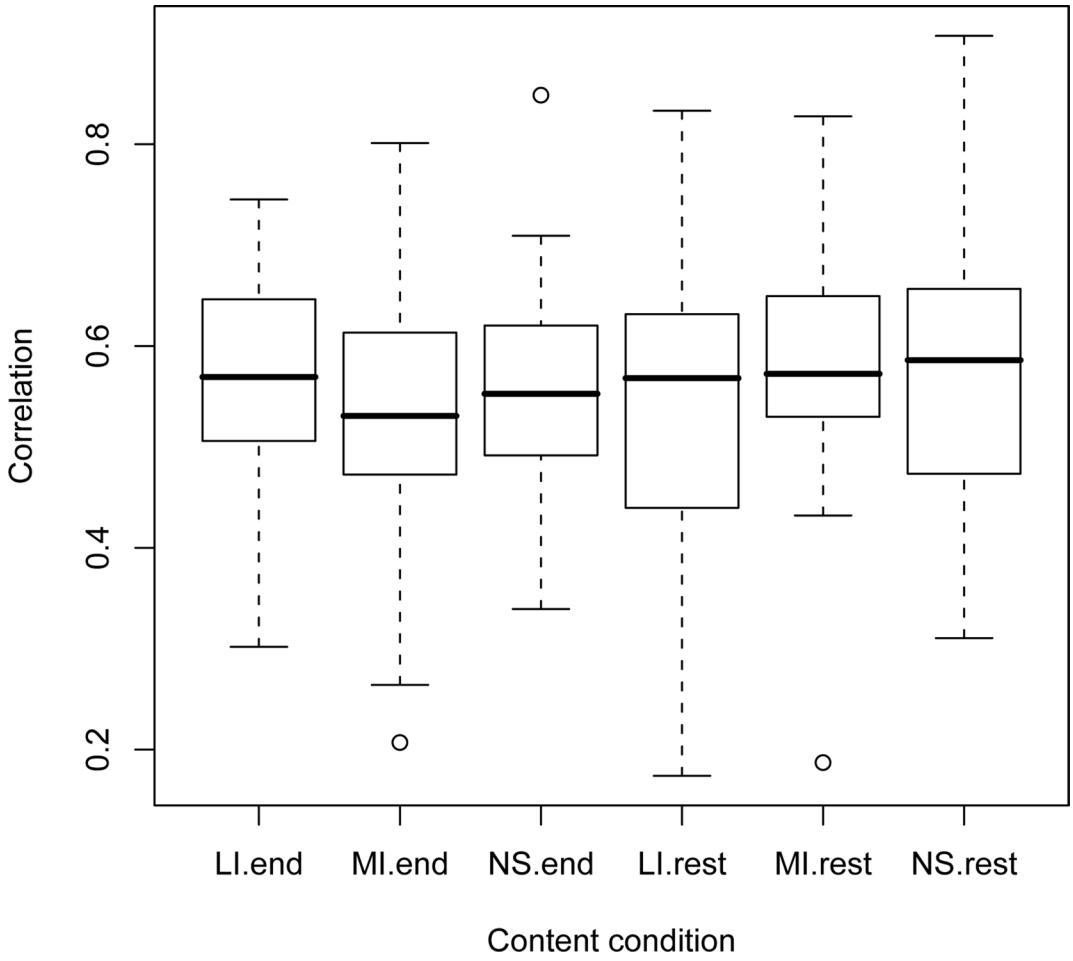

Fig. S5. Correlation between the 2 seed regions in each of the 6 experimental conditions. The figure shows the distribution of correlation values across participants, per experimental condition. LI, less informative; MI, more informative; NS, nonnarrative sentence conditions. ''End'' refers to connectivity during listening; ''Rest'' refers to connectivity during rest periods after listening.

Table S1. Regions showing differential connectivity during listening and rest

Region	BA	fROI no. (Fig. 1)	TLRC coordinates		
			X	Y	Z
Left hemisphere					
Frontal					
PreCG	4	2	−27	−27	56
PreCG	6	4	−45	−4	34
PreCG	6	13	−41	−12	32
PreCG	44/6	17	−49	2	8
PreCG	6	22	−26	−14	59
MedFG	6	5	−7	−8	60
MFG	6	6	−36	1	49
MFG	9	16	−36	12	32
MFG	10	21	−39	45	20
IFG	46	18	−45	17	25
SFG	6	20	−6	8	65
SFG	6	23	−7	27	56
Temporal					
STG	21	1	−50	−21	2
MTG	19	24	−45	−60	15
Insula					
Claustrum/insula		7	−33	−12	11
Insula	13	25	−43	−12	17
Postcentral					
PoCG	3	8	−26	−37	46
PoCG.	2	14	−53	−18	27
PoCG	2	15	−24	−34	60
PoCG	3	19	−44	−21	53
Midline					
PCL	31/24	3	−10	−16	45
PCL	4	12	−7	−36	64
Cingulate G.	31	9	−13	−42	32
Caudate/anterior cingulate		10	−15	18	14
Cuneus	18/17	11	−1	−77	14
Cuneus	17	26	−21	−81	11
Right hemisphere					
Frontal					
MedFG	6	2	7	−13	57
PreCG	6	3	42	−10	43
PreCG	4	4	26	−27	57
Temporal					
STG	41	1	49	−28	7
Postcentral					
PoCG	5	6	23	−39	60
PoCG	7	13	12	−47	65
PoCG	7	16	20	−50	65
Midline					
Cuneus	18	5	13	−69	19
PCL/cuneus	5	7	10	−33	47
Caudate/anterior cingulate		8	11	24	11
PCun	31	9	26	−75	18
PCun	7	14	5	−48	53
PCgG	30	10	21	−59	8
PCgG	23	11	6	−52	20
PCgG	30	15	17	−46	11
Lingual G.	18	12	16	−68	5

fROI no. refers to location of these clusters as numbered in Fig. 1.

Table S2. Regions demonstrating differential functional connectivity (FC) with both seed regions as a function of content

Region	BA	fROI no.	TLRC coordinates		
			X	Y	Z
Content-sensitive FC collapsed across listening and rest (fROI no. in Fig. 2)					
L. PreCG.	6	1	−48	−9	30
L. PreCG.	4	2	−25	−30	56
R. cingulate G.	23	3	6	−48	26
R. SFG	9	4	16	35	37
Content-sensitive FC during rest (fROI no. in Fig. S2)					
L. PreCG	6	1	−48	−8	31
L. PreCG	6	2	−18	−17	65
R. SFG	8	3	11	39	40
R. PCgG	23	4	7	−48	25
R. PreCG	6	5	52	−5	30
R. PreCG	40	6	34	−36	53